

Full Paper

Fragment-Based Design, Synthesis, and Biological Evaluation of 1-Substituted-indole-2-carboxylic Acids as Selective Mcl-1 Inhibitors

Ziqian Wang^{1*}, Wenjie Xu^{1*}, Ting Song², Zongwei Guo², Lu Liu¹, Yudan Fan², Anhui Wang¹, and Zhichao Zhang¹¹ State Key Laboratory of Fine Chemicals, School of Chemistry, Dalian University of Technology, Dalian, People's Republic of China² School of Life Science and Technology, Dalian University of Technology, Dalian, People's Republic of China

Based on a known selective Mcl-1 inhibitor, 6-chloro-3-(3-(4-chloro-3,5-dimethylphenoxy)propyl)-1*H*-indole-2-carboxylic acid, we applied a fragment-based approach to obtain new molecules that extended into the p1 pocket of the BH3 groove and then exhibited binding selectivity for the Mcl-1 over the Bcl-2 protein. After we deconstructed the 1*H*-indole-2-carboxylic acid from the parental molecule, a benzenesulfonyl was substituted at the 1-position to adopt a geometry preferred for accessing the p1 pocket according to the binding mode of the parental molecule identified by X-ray crystallography. A linear relationship between the free energy of ligand binding (ΔG) and the count of non-hydrogen heavy atoms (HAC) was maintained during the molecular growing to occupy the p1 pocket. Finally, we not only obtained compound **12** with a 7.5-fold selectivity to Mcl-1 ($K_i = 0.48 \mu\text{M}$ by fluorescence polarization) over Bcl-2 ($K_i = 3.6 \mu\text{M}$), but also provided evidence that additional occupation of the p1 pocket is more favorable for Mcl-1 than for Bcl-2 binding, and contributes more to Mcl-1 inhibition than occupation of the p2 pocket. Compound **12** exhibited a selective killing ability on Mcl-1-dependent cancer cells.

Keywords: Fragment-based drug design / Ligand efficiency / Mcl-1 inhibitor / p1 pocket / Selective

Received: August 30, 2016; Revised: November 8, 2016; Accepted: November 9, 2016

DOI 10.1002/ardp.201600251



Additional supporting information may be found in the online version of this article at the publisher's web-site.

Introduction

Mediated by the BH3 domain shared by both anti-apoptotic (Bcl-2, Bcl-x_L, Mcl-1, etc.) and pro-apoptotic (multi-domain proteins Bax and Bak, and BH3-only proteins) members, the Bcl-2 family proteins form heterodimers to play a key role in regulation of apoptotic pathways [1, 2]. The BH3 domain of

pro-apoptotic proteins possesses four conserved hydrophobic residues that insert into four hydrophobic sub-pockets, p1–p4, in the BH3-binding groove of anti-apoptotic proteins, while an aspartate makes a salt bridge with a conserved arginine residue on anti-apoptotic members [3, 4].

The anti-apoptotic Bcl-2 proteins are overexpressed in a large number of tumors preventing cells from undergoing apoptosis [5]. They are thus attractive yet challenging targets for developing new anticancer therapies [1, 6, 7]. The BH3 binding groove of Bcl-2 and Bcl-x_L are the primary focus for the design of Bcl-2 inhibitors [8]. The specific Bcl-2/Bcl-x_L

Correspondence: Dr. Zhichao Zhang, State Key Laboratory of Fine Chemicals, School of Chemistry, Dalian University of Technology, Dalian 116012, People's Republic of China.

E-mail: zczhang@dlut.edu.cn**Fax:** +86-411-84986032

*These authors contributed equally to this work.

inhibitor Navitoclax is currently in phase I/II clinical trials [9, 10]. However, the cancer killing ability of Navitoclax based on disruption of the heterodimers between anti-apoptotic and pro-apoptotic Bcl-2 members is limited to Bcl-2-dependent tumors and it is encountering resistance in Mcl-1 expressing cancer cells [11, 12].

Mcl-1 protein possesses an overall similar but divergent BH3-binding groove compared with Bcl-2 and Bcl-x_L, which exhibits unique anti-apoptotic functions. Mcl-1 has been documented as the other arm of the antiapoptotic Bcl-2 family to help cancer evade apoptosis [13]. So far, nine series of selective Mcl-1 inhibitors that were predicted and/or identified to bind in the BH3-binding groove of Mcl-1 have been investigated by Wang, Fesik, Zaneta Nikolovska-Coleska, our group, and others since 2012 [14, 15]. However, structural insights into features that contribute to Mcl-1 binding selectivity and affinity are still elusive. Most of these known selective Mcl-1 inhibitors focused on the optimization of p2 occupation because it is the deepest and largest sub-pocket among four sub-pockets in BH3-binding groove of Mcl-1 and it showed some plastic property that distinguishes Mcl-1 from the corresponding one on Bcl-2/Bcl-x_L. By contrast, p4 was not a favorable pocket for Mcl-1 binding selectivity [14]. Of note, neither the reported selective Mcl-1 inhibitors nor Bcl-2/Mcl-1 dual inhibitors explore the p1 pocket although this pocket could be involved in substrate binding energy improvement.

Most of the known selective Mcl-1 inhibitors or their parental leads were obtained from HTS (high-throughput screening) or found by accident. The others were developed by fragment-based drug design (FBDD), in which a minimal binding fragment was discovered through NMR-based screening or deconstruction from a known inhibitor [14]. With the aid of structure-based drug design, the final drug-like candidates were obtained through fragment growing, linking, or scaffold merging to markedly increase the affinity of the starting fragments [16]. FBDD has been rapidly developed over the past decades and showed significant advantages over HTS [17, 18]. ABT-737, the parental molecule of Navitoclax, was also discovered by this strategy [19]. It is necessary to obtain the structural binding information of the starting fragment for the further optimization by exploiting the structure–activity relationship analysis (SAR) observed during molecular evolution [20, 21]. Additionally, the conservation of binding mode during molecular growing could be reflected by a linear relationship between molecular weight and binding affinity. The prediction map would provide critical and quantitative assessments to guide the future drug development [22–24].

Here, we chose a fragment from a known molecule that has been identified by X-ray studies to bind Mcl-1 selectively and its relatively high ligand efficiency (LE) value could guarantee the binding mode conservation. With the aid of structure-based drug design, a series of inhibitors that engaged into the p1 pocket was obtained through fragment growing. A linear relationship between ΔG and HAC was well maintained

during the molecular growing to progressively occupy p1 pocket. Finally, we not only obtained compound **12** with a 7.5-fold selectivity to Mcl-1 over Bcl-2, but also provided an evidence that occupation of the p1 pocket is more favorable for Mcl-1 binding than Bcl-2, and contributes more to Mcl-1 inhibition than occupation of the p2 pocket.

Results and discussion

Rationale

According to the mutation studies of Bcl-2 and Mcl-1 in complex with BH3 peptide, respectively, together with our previous finding in SAR studies of Bcl-2/Mcl-1 dual inhibitors, mimicking D67 of Bim BH3 peptide to capture a conserved R146 or R263 is a widely recognized molecular basis to confer a major binding energy to a molecule binding either Bcl-2 or Mcl-1 [25]. Additionally, eight of nine series reported selective Mcl-1 inhibitors could form a hydrogen bond with R263 and/or N260 on Mcl-1 protein [14, 15]. We then decided to maintain the interactions with R263 to contribute binding energy when we designed new selective Mcl-1 inhibitors.

With respect to the four hydrophobic pocket p1, p2, p3, and p4, we focused on the p1 pocket because we found significant features that might be exploited to contribute Mcl-1 selectivity. First, the p1 of Mcl-1 is not as open as that in Bcl-2/Bcl-x_L because the α -helix 3 is well formed in the Mcl-1 complex but poorly formed in the Bcl-2 complex (Fig. 1). Second, the p1 and p2 pockets are less contiguous in Mcl-1 than that in Bcl-2 when complexed with Bim because M231, a

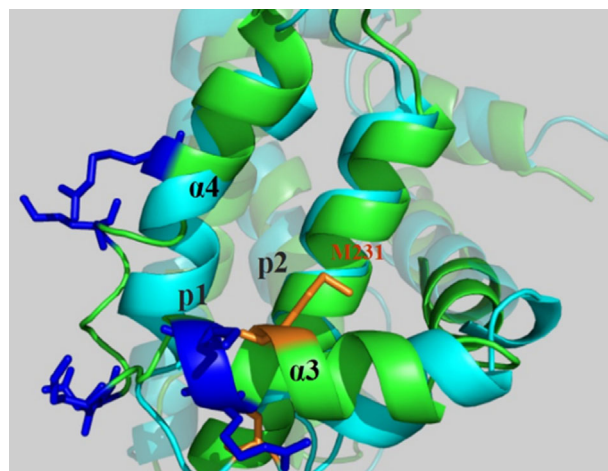


Figure 1. Overlay of Mcl-1 from the Mcl-1BLR:hBim BH3 complex (PDB ID: 2PQK, green) and Bcl-2 from Bcl-2:Bim BH3 complex (PDB ID: 4B4S, light blue). M231 on Mcl-1 that is located between p1 and p2 and the corresponding Y59 of Bcl-2 were highlighted in orange. Positively charged residues on Mcl-1 that construct the p1 pocket was marked with dark blue.

residue located between p1 and p2, is more solvent exposed on Mcl-1 than the corresponding Y59 on Bcl-2. Third, the surface of Mcl-1 is more electropositive than that of other Bcl-2 proteins. In particular, as showed in Fig. 1, a number of positively charged residues are present on α -helix 3, the α -helix 3 to α -helix 4 loop, and α -helix 4 in Mcl-1, which construct the p1 pocket [26]. These differences in p1 pocket may contribute to a specific binding properties of Mcl-1. Additionally, p1 is much narrower than p2, which may provide more potency for additional substituents to expand the occupation. The known nine series of selective Mcl-1 inhibitors and all the pan-Bcl-2 inhibitors do not thus far explore the p1 pocket.

Here, we choose 1-methyl-indole-2-carboxylic acid (compound **1**, compound **13** in original literature) as the starting fragment [27]. **1** exhibited a K_i value of 160 μ M to bind Mcl-1 and its binding position in BH3-binding groove of Mcl-1 has been identified by X-ray studies of its analogs, showing that the carboxylic acids of **1** interact with R263 of Mcl-1 and the indole core could stably locate at the p2 pocket during the following molecular merge. Further, suitable substituents at 1-position of 1*H*-indole-2-carboxylic acid was designed to access the p1 pocket (Supporting Information Fig. S1).

Chemistry

Compound **2** was prepared by benzenesulfonyl chloride and methyl indole-2-carboxylate according to literature procedures [28]. Then, analogs **3–6** were synthesized in which the 4-position of phenylsulfonyl moiety was replaced with $-\text{Ph}$, $-\text{O-Ph}$, $-t\text{-Amyl}$, and $-\text{O-}i\text{-Bu}$, respectively. These analogs were prepared by a four-step synthesis, as shown in Scheme 1. 4-substituted benzenesulfonic acids were prepared by commercially available substituted benzenes and ClSO_3H [29]. They were then converted to the corresponding sulfonyl chlorides by SOCl_2 [30]. The amidation reaction with methyl indole-2-carboxylate and subsequent ester hydrolysis with LiOH yielded final compounds **3–6**.

Compounds **7–12** were synthesized by a different four-step synthesis, as shown in Scheme 2. The *O*-substituted sodium 4-hydroxybenzenesulfonates were prepared by benzylation

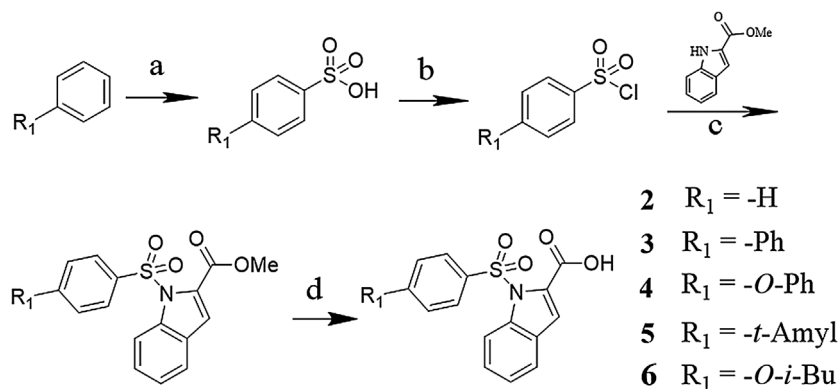
of sodium 4-hydroxybenzenesulfonate with different substituted benzyl bromides [31]. Reaction of sodium salt with SOCl_2 in DMF afforded sulfonyl chloride which was coupled with methyl indole-2-carboxylate in DMF to give the corresponding methyl esters of **7–12**. Alkaline hydrolysis of these esters yielded carboxylic acids **7–12** [32].

Structure-based design, synthesis, and active evaluation

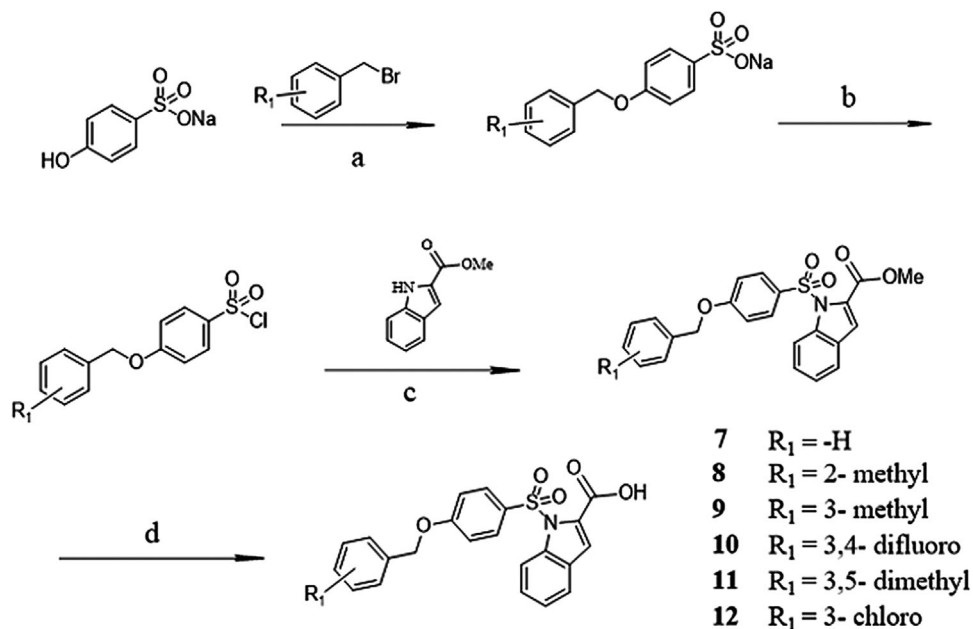
Based on the binding mode of compound **1** and our aims, a benzenesulfonyl was substituted at 1-position because a sulfonamide moiety could adopt an appropriate geometry for engaging into the p1 pocket as it may be oriented in parallel with the groove. Chemical accessibility was also taken into account. 1-(Phenylsulfonyl)-1*H*-indole-2-carboxylic acid (**2**) was then obtained.

The binding affinity (K_i value) of **2** was evaluated using fluorescence polarization assays (FPA), which measured its ability to competitively displace a Bid-derived peptide from Mcl-1/Bcl-2. *R*-(-)-Gossypol was used as a positive control. It was found that **2** binds to Mcl-1 with a threefold affinity improvement than compound **1** ($K_i = 50 \mu\text{M}$ vs. 160 μM) toward Mcl-1. A K_i value of 80 μM for **2** binding to Bcl-2 protein was also found (Table 1).

Next, a heteronuclear single quantum coherence (HSQC) NMR spectroscopy experiment using ^{15}N labeled Mcl-1 protein validated our design strategy. Figure 2a shows a plot of the chemical shift perturbations against the overall Mcl-1 protein residues. Approximately 65% of the residues that were perturbed above the threshold value (0.06 ppm) were located in the p2 pocket. Compared with the residues affected by compound **1** in the previous report, the residues of R263, L267, F270, A271, A227, and F228 exhibited a similar chemical shift upon the addition of compound **2**. Moreover, M231, L232, L246, V249, and V253 are newly emergent residues with significant chemical shift ($\Delta\text{CS} > 0.07 \text{ ppm}$), and these residues are closer to the p1 pocket than the above-mentioned residues. The NMR-derived models (Fig. 2b) demonstrate that the indole core keeps the original binding mode of the



Scheme 1. Synthesis of compounds **3–6**. Reagents and conditions: (a) ClSO_3H , dry CHCl_3 , ice-water bath, nitrogen atmosphere protection, 1.5 h; (b) SOCl_2 , two drops DMF, 80°C, 2 h; (c) NaH , dry DMF, room temperature, 1 h; (d) LiOH , MeOH/THF/water , 70°C, 5 h; HCl , $\text{pH} = 2$.



Scheme 2. Synthesis of compounds 7–12. Reagents and conditions: (a) substituted benzyl bromide, 1 N NaOH, isopropanol, 75°C, 20 h; (b) SOCl₂, dry DMF, 5 min; ice water, 5 min; (c) NaH, dry DMF, room temperature, 1 h; (d) LiOH, MeOH/THF/water, 70°C, 5 h; HCl, pH = 2.

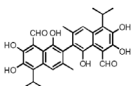
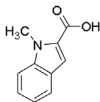
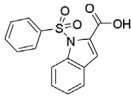
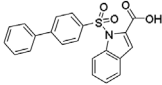
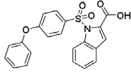
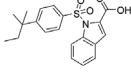
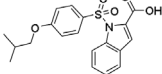
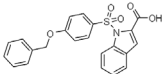
starting fragment, and benzenesulfonyl orients toward the p1 pocket. We proposed that elaboration at *para* position of benzenesulfonyl with hydrophobic substitutions could probe the p1 pocket and then achieve further gains in affinity and selectivity.

Compound 3, with a further elongation of benzenesulfonyl, showed a similar fivefold affinity improvement toward both Mcl-1 and Bcl-2 compared with 2 ($K_i = 9.8$ and $19.3 \mu\text{M}$, respectively). A twofold selectivity between Bcl-2 and Mcl-1 was observed for compound 3. Encouraged by the binding improvement of 3, and to further improve the selectivity between Mcl-1 and Bcl-2, we tried to increase the Mcl-1 affinity by fitting the steric hindrance of the specific M231 in the p1 of Mcl-1. Compounds 4, 5, 6, and 7 with oxygen atom as a linker or alkyl substituents of various sizes at the *para* position of the benzenesulfonyl were prepared to obtain proper length and flexibility for substituent to adapt to p1. From this set of compounds, a trend emerged showing much improved Mcl-1 affinity than Bcl-2 that compound 7 exhibited a 6.5-fold selectivity for binding to Mcl-1 ($K_i = 1.3 \mu\text{M}$) over Bcl-2 ($K_i = 8.3 \mu\text{M}$).

Consequently, analogs with different substituents at *o*-, *m*-, *p*-position of benzyloxy were prepared to further probe the p1 pocket, yielding compounds 8–12 (Table 2). According to FPA, although compounds 8 and 9 with 2- or 3-methyl substituted showed improvement in affinity, they increased equally against Bcl-2 and Mcl-1 compared with compound 7. An obvious loss of selectivity between the two proteins was

even found for compound 10 with larger hindrance of 3,5-dimethyl-substitution, most likely due to the wider p1 pocket of Bcl-2 than that of Mcl-1 as showed in Fig. 1. To improve the selectivity, we then substituted difluoro and chlorine with small size to yield compounds 11 and 12. Additionally, we suspected that these polar moieties might interact with the more positive Mcl-1 surface better than Bcl-2. As expected, compound 12 showed a 7.5-fold selectivity to bind Mcl-1 ($K_i = 0.48 \mu\text{M}$) over Bcl-2 ($K_i = 3.6 \mu\text{M}$). To test if the binding site of compound 12 maintained the original fragment in the p2 and extended into p1 as we suspected, ¹H-¹⁵N HSQC NMR spectroscopy studies were performed. The chemical shift changes in the presence of 12 were mapped and plotted against Mcl-1 residues (Fig. 3a). Chemical shift perturbations of F228, L232, L246, V249, V253, L267, F270, and R263 which located at the p2 pockets were also observed as caused by compound 2. Moreover, L232, L235, D236, V243, K244, S245 located on α -helix 3 and 4 that construct p1 are newly emergent residues with significant chemical shift perturbations ($\Delta\text{CS} > 0.065 \text{ ppm}$) caused by compound 12, indicating that 12 did extend deeply into the p1 pocket. I237, K238, N239, and D242 that located on an unstructured loop connecting α -helix 3 and α -helix 4 and surrounded p1 also showed significant chemical shift perturbations ($\Delta\text{CS} > 0.06 \text{ ppm}$). NMR-derived structure of 12 bound to Mcl-1 is shown in Fig. 3b. We then overlay the compound 12 and α -helix in Bim. As shown in Fig. 3c, 12 mimics D67 to maintain the interaction with R263 as its starting fragment compound 1

Table 1. Fragment 1 and its derivatives: Name, structure, and binding affinity determined by fluorescence polarization assays (FPA).

Compounds	Structure	K_i (μM)	
		Mcl-1	Bcl-2
<i>R</i> -(–)-Gossypol		0.19 ± 0.01	0.32 ± 0.01
1		160	ND
2		50 ± 5.70	80 ± 7.38
3		9.8 ± 0.73	19.3 ± 1.21
4		6.3 ± 0.43	17.2 ± 0.97
5		4.8 ± 0.40	11.6 ± 0.88
6		5.9 ± 0.44	14.5 ± 0.62
7		1.3 ± 0.25	8.3 ± 0.45

does, and it mimics L62 and I58 hotspots simultaneously. It could explore the p1 as deep as the I58 of Bim could reach.

To further characterize the binding affinities of the compounds to Mcl-1 and Bcl-2, we applied an enzyme-linked immunosorbent assay (ELISA) for compounds **7**, **10**, and **12**. As shown in Table 3, compounds **7** and **10** exhibited 6.2-fold and 10.8-fold selectivity for binding to Mcl-1 over Bcl-2, while compound **8** exhibited only 4.3-fold selectivity. These data were consistent with the FP results.

To our knowledge, compounds **2–12** are the first series of I58 mimicking inhibitors that developed by fragment-based strategy to extend a starting fragment into the p1 pocket. Thus, this is a promising series to study the contribution of p1 pocket to Mcl-1 binding. We then plotted the ΔG of these inhibitors against the HAC to monitor the efficiency during fragment growing. As shown in Fig. 4a (Supporting Information Table S1), a linear ($R^2=0.9$) relationship

between ΔG and HAC was found for compounds **2–12**, indicating the conservation of the binding mode upon elaboration of the starting fragment. The parental 1*H*-indole-2-carboxylic acid core constantly remained interaction with R263 in Mcl-1 and the 1-position substituent access an additional p1 pocket. Moreover, a different slope was found for the growing path toward different targets. Each additional heavy atom contribute approximately $0.27 \text{ kcal mol}^{-1}$ energy to Mcl-1, while a minor one was found for Bcl-2 which is $0.17 \text{ kcal mol}^{-1}$. It illustrated that the occupation of p1 pocket is more favorable for binding Mcl-1 than Bcl-2. We then plotted the molecular weight (MW) against the pK_i ($-\log K_i$) to further quantify this differences (Fig. 4b, Supporting Information Table S1). The trend line with a value for the slope of 61, implied by the compounds' data, along with the path of ideal optimization, showed that an increase of 1 pK_i unit can be expected for every 61 mass units added to the

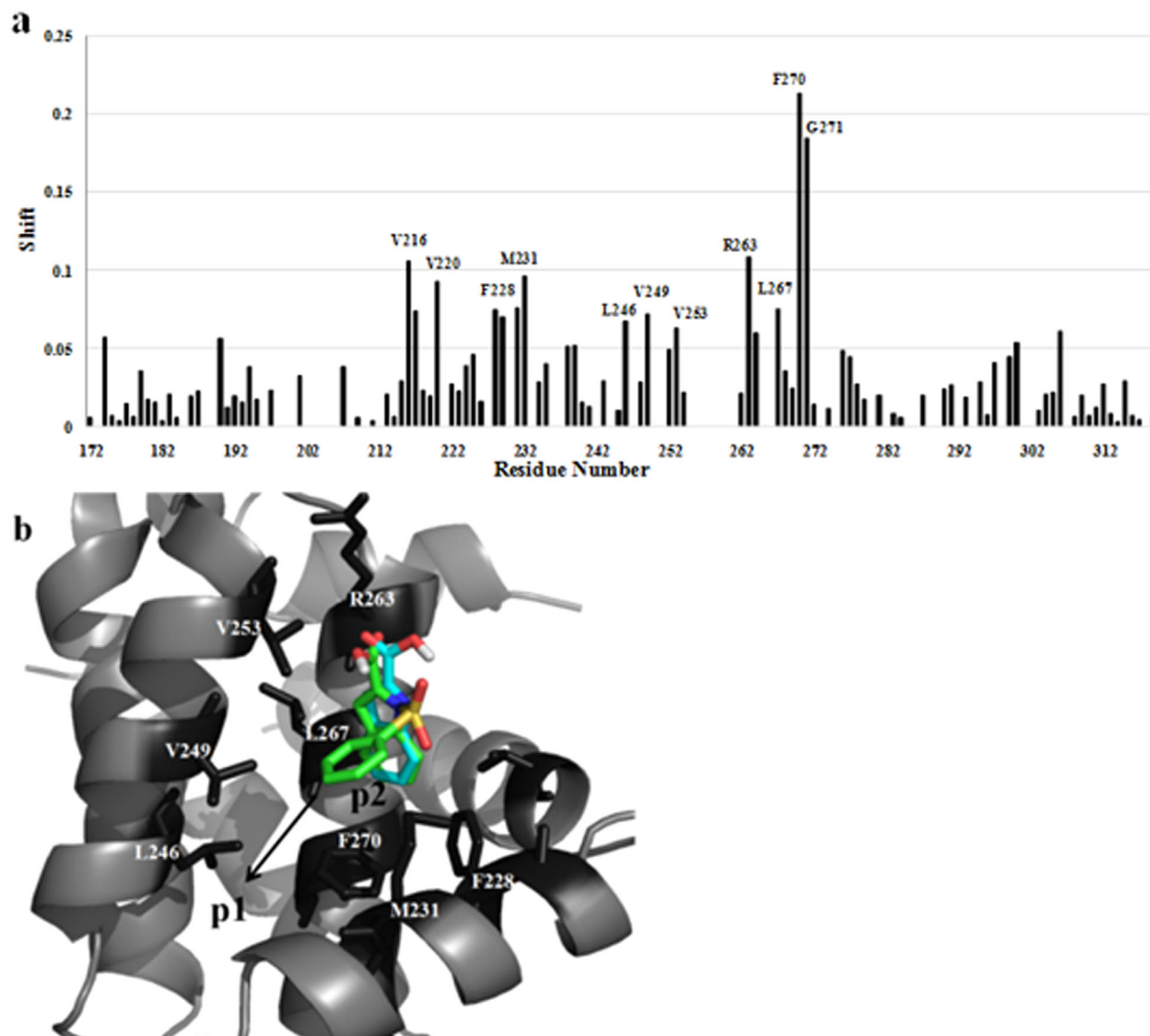


Figure 2. (a) Chemical shift perturbations of Mcl-1 residues bound to compound 2. (b) Mcl-1 residues shown to be perturbed in HSQC NMR in the presence of 2 (green).

compound. For Bcl-2 protein, the value for the slope increased to about 87.

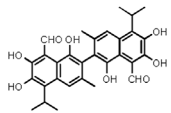
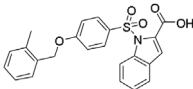
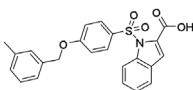
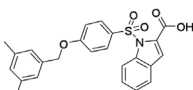
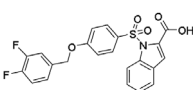
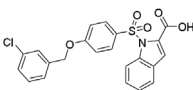
Furthermore, we compared our optimization process to other seven known Mcl-1 selective inhibitors, all of which are optimized for p2 occupation (Supporting Information Table S2). The present compounds in this study showed more binding efficiency than other five series (Fig. 5a). We analyzed the MW/ pK_i curve of molecules previously (Fig. 5b). The average value of the slope of the trend line is around 85. That is, for those molecules optimized toward p2 occupation, an increase of 1 pK_i unit can be expected for every 85 mass units added to the compound. Therefore, optimization for p1

occupation is an effective way to increase Mcl-1 binding affinity of designed compounds.

Compound 12 selectively induces apoptosis in Mcl-1-dependent cancer cells

To confirm the specificity of 7, 10, 12 for Mcl-1 protein in cellular models, we analyzed its activity in four cell lines (Fig. 6 and Supporting Information Fig. S2). NCI-H23 cells depend on Mcl-1 for survival. In contrast, HL-60 cells are Bcl-2-dependent cells and H22 and MCF-7 cells are dependent on both Mcl-1 and Bcl-2. Figure 6a showed Western blot analysis of the

Table 2. Compounds 8–12: Name, structure, and binding affinity by FPA (K_i , μM).

Compounds	Structure	K_i (μM)	
		Mcl-1	Bcl-2
R-(–)-Gossypol		0.19 ± 0.01	0.32 ± 0.01
8		0.73 ± 0.12	5.2 ± 0.17
9		0.75 ± 0.08	5.3 ± 0.23
10		0.65 ± 0.04	2.8 ± 0.03
11		0.64 ± 0.03	4.7 ± 0.03
12		0.48 ± 0.01	3.6 ± 0.02

expression levels of Bcl-2 and Mcl-1 in these cell lines. These cell lines were treated with different concentrations of **12**, and then apoptosis was determined by Annexin V flow cytometry. After 48 h treatment, **12** induced apoptosis in NCI-H345 cells ($\text{IC}_{50} = 2.2 \mu\text{M}$), which was 30-fold greater than that in HL-60 cells ($\text{IC}_{50} = 63.3 \mu\text{M}$), consistent with its binding selectivity for Mcl-1 over Bcl-2. The activity of **12** in H22 ($\text{IC}_{50} = 9.2 \mu\text{M}$) cells and MCF-7 cells ($\text{IC}_{50} = 19.2 \mu\text{M}$) was not as sensitive as that in NCI-H23 cells (Fig. 6b). Furthermore, compound **10**, with less selectivity for Mcl-1 over Bcl-2, induced potent apoptosis in both NCI-H345 ($\text{IC}_{50} = 8.7 \mu\text{M}$) and HL-60 cells ($\text{IC}_{50} = 23.1 \mu\text{M}$), while the less potent compound **7** failed to sensitively induce apoptosis in both of the cell lines (Supporting Information Fig. S2).

Conclusion

Following a fragment-based strategy and structure-based design, we not only obtained compound **12** that exhibits 7.5-fold binding selectivity toward Mcl-1 ($K_i = 0.48 \mu\text{M}$ by FP) over Bcl-2 ($K_i = 3.6 \mu\text{M}$), but also obtained a series of small molecule tools to explore the p1 pocket of BH3-binding groove on both Mcl-1 and Bcl-2. Through analysis of $\Delta G/\text{HAC}$

and MW/pK_i of these molecules against the two proteins, we found that the p1 occupation exhibits a higher efficiency for binding Mcl-1 than occupation of p2, and it is more favorable for Mcl-1 inhibition than that for Bcl-2 inhibition. Our evidence illustrated that the p1 could be a key binding site for selective Mcl-1 inhibitor design.

Experimental

Chemistry

General

All commercial reagents were purchased and used without further purification or distillation unless otherwise stated. ^1H NMR spectra was recorded on a Bruker AV-500 spectrometer using DMSO as solvent. Chemical shifts were reported in δ values (ppm) with tetramethylsilane as the internal reference, and J values were reported in hertz (Hz). The following abbreviations are used for multiplicity of NMR signals: s = singlet, d = doublet, t = triplet, q = quartet, m = multiplet. High-resolution mass spectra (HRMS) were obtained on HPLC-Q-ToF MS (Micro) spectrometer. Column chromatography was performed on silica gel 200–300 mesh.

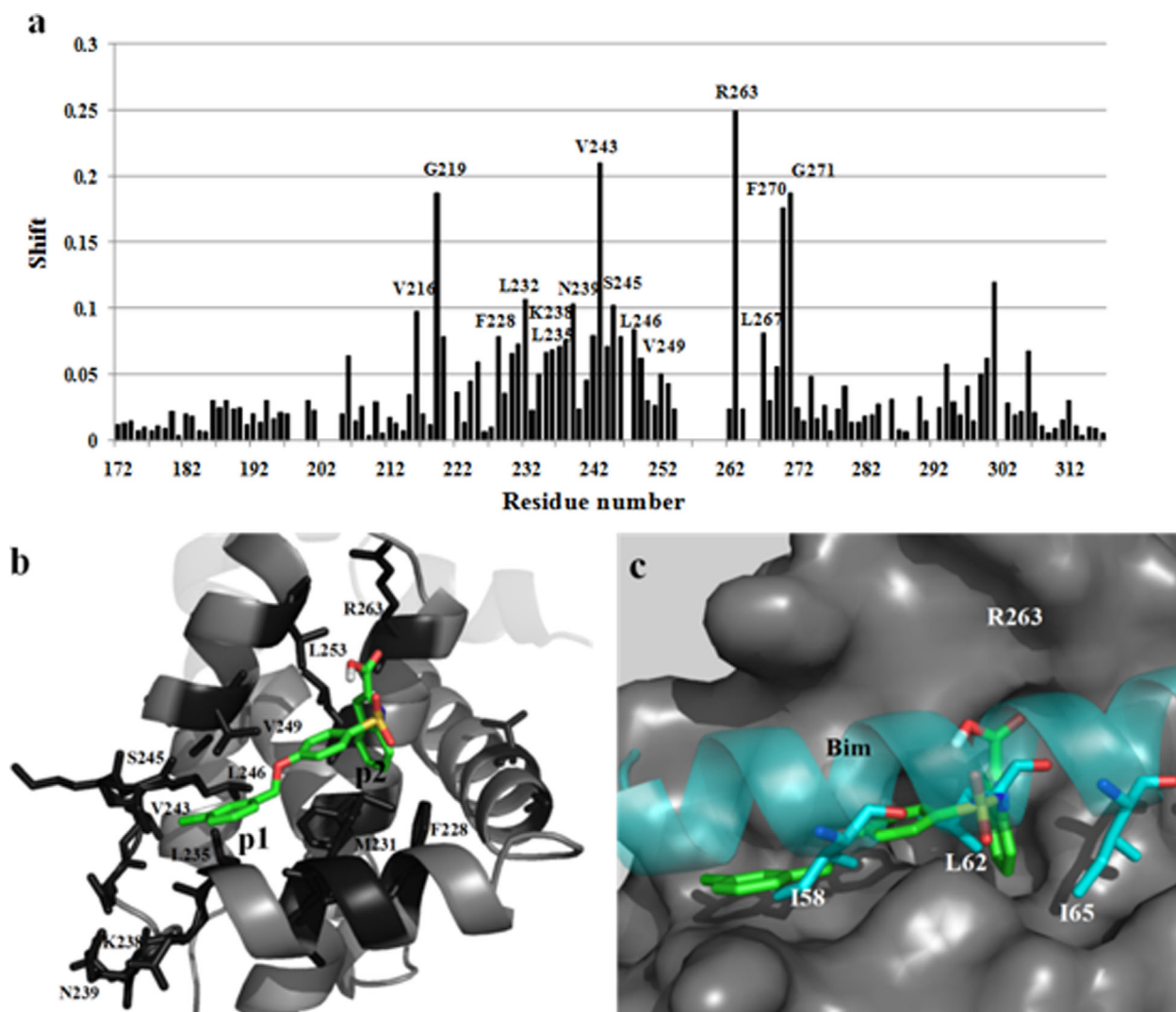


Figure 3. (a) Plot of chemical shift changes of Mcl-1 amide upon addition of **12** (Mcl-1:**12** = 1:2) as a function of Mcl-1 residue numbers. (b) Mcl-1 residues shown to be perturbed in HSQC NMR in the presence of **12** (green). Significant shift ($\Delta CS > 0.06$ ppm) including R263, M231 in p2, and the residues L235, V243, K238, and N239 in the p1 pocket are highlighted in dark gray. (c) Side view of **12** bound to Mcl-1 overlaid with the bound Bim peptide.

Table 3. Competitive binding of **7**, **10**, and **12** to Mcl-1 and Bcl-2 protein determined by ELISA assay (IC_{50} , μM).

Compounds	IC_{50} (μM)	
	Mcl-1	Bcl-2
<i>R</i> -(–)-Gossypol	0.35 ± 0.14	0.72 ± 0.07
7	3.0 ± 0.3	18.6 ± 1.1
10	1.2 ± 0.32	5.2 ± 0.5
12	0.75 ± 0.18	9.6 ± 0.8

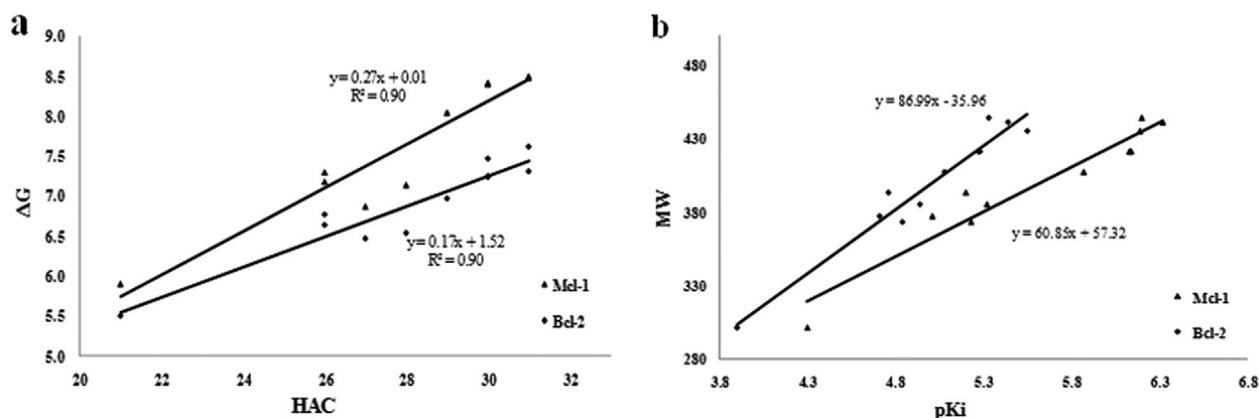


Figure 4. (a) ΔG (in kcal mol⁻¹) of compounds 2–12 plotted as a function of HAC in the compounds toward Mcl-1 and Bcl-2, respectively. (b) Linear relationship between MW and p*K*_i of compounds 2–12 toward Mcl-1 and Bcl-2, respectively.

The InChI codes of the investigated compounds together with some biological activity data are provided as Supporting Information.

1-(Phenylsulfonyl)-1*H*-indole-2-carboxylic acid (2)

Yield: white solid, 460 mg, 85%. ¹H NMR (500 MHz, DMSO) δ : 11.74 (s, 1H), 8.02 (d, *J* = 12.0 Hz, 2H), 7.67 (m, *J* = 7.5 Hz, 4H), 7.49–7.41 (m, 1H), 7.36–7.30 (m, 2H), 7.23 (t, *J* = 7.5 Hz, 1H), 7.06 (dd, *J* = 13.9, 6.0 Hz, 1H). TOF MS (EI⁺): C₁₅H₁₁NO₄S, found 301.04.

General procedure for the preparation of compounds 3, 4, 5, and 6

The general procedure is illustrated immediately below with compound 3 as a specific example.

Synthesis of (1,1'-biphenyl)-4-sulfonic acid. Biphenyl (3.08 g, 20 mmol) was dissolved in chloroform (150 mL). Chlorosulfonic acid (1.31 mL, 20 mmol) in 25 mL chloroform was added dropwise over 30 min under an ice-water bath and a nitrogen atmosphere protection. With the addition of chlorosulfonic acid, a white solid precipitated gradually. The reaction mixture was stirred for further 1 h, then the precipitate was collected by filtration and washed with cold chloroform. Yield: 2.8 g, 60%.

Synthesis of (1,1'-biphenyl)-4-sulfonyl chloride. (1,1'-Biphenyl)-4-sulfonic acid (2.8 g, 12 mmol) was dissolved in dichloro sulfoxide (25 mL) and treated with a catalytic amount of *N,N*-dimethylformamide (two drops). The mixture was heated at 80°C for 2 h. After the completion of the reaction, the mixture was concentrated *in vacuo*. The residual thionyl chloride was

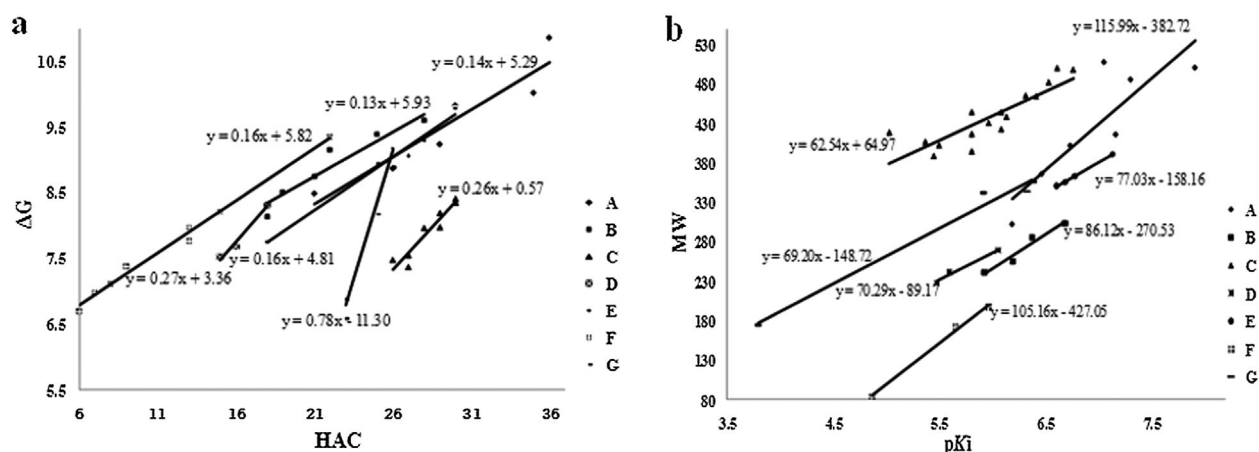


Figure 5. (a) ΔG (in kcal mol⁻¹) for series of A–G plotted as a function of HAC in the compounds toward Mcl-1 protein. (b) Linear relationship between MW and p*K*_i of series of A–G toward Mcl-1 protein.

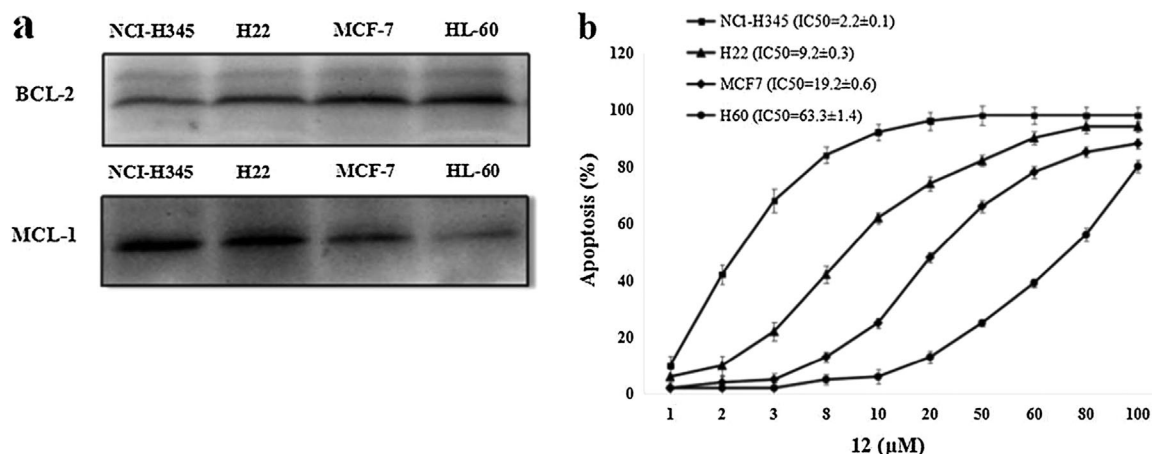


Figure 6. (a) The levels of Mcl-1 and Bcl-2 protein in NCI-H23, H22, MCF-7, and HL-60 cells were examined by Western blot. (b) Cells were treated with graded concentration of 12 for 48 h, and the percentage of apoptotic cells was determined by Annexin V flow cytometry.

removed by toluene (15 mL × 3) under the condition of vacuum. Yield: 2.4 g, 80%.

Synthesis of methyl 1-((1,1'-biphenyl)-4-ylsulfonyl)-1H-indole-2-carboxylate. The NaH (60%, 632 mg, 15.8 mmol) was added in three portions to a solution of methyl 1H-indole-2-carboxylate (1.1 g, 6.3 mmol) in dry *N,N*-dimethylformamide (10 mL) under stirring at room temperature for 1 h, then (1,1'-biphenyl)-4-sulfonyl chloride (2.4 g, 9.5 mmol) was added to this mixture. After 1 h, the solution was poured into 20 mL cooled water. The resulting precipitate was filtered and purified by silica gel chromatography (ethyl acetate/petroleum ether = 1:6) to generate 1.6 g of the product as the white powder solid. Yield: 65%.

Synthesis of 1-((1,1'-biphenyl)-4-ylsulfonyl)-1H-indole-2-carboxylic acid (3). To a solution of methyl 1-(phenylsulfonyl)-1H-indole-2-carboxylate (1.6 g, 4.1 mmol) in tetrahydrofuran/methanol/water (5:5:1, 22 mL) was added lithium hydroxide monohydrate (688 mg, 28.7 mmol). The reaction mixture was heated at 70°C for 5 h. After cooling to room temperature, it was concentrated, followed by addition of water (10 mL). The pH was adjusted to 2 with 1 N HCl and extracted with ethyl acetate (15 mL × 3). The combined extraction was dried over anhydrous sodium sulfate, filtered, and concentrated. The crude product was purified by recrystallization in a mixture of dichloromethane and hexanes to afford compound 3 as white solid.

1-((1,1'-Biphenyl)-4-ylsulfonyl)-1H-indole-2-carboxylic acid (3)

Yield: white solid, 2.11 g, 28%. ¹H NMR (500 MHz, DMSO) δ: 11.74 (s, 1H), 8.09 (dd, *J* = 24.7, 8.5 Hz, 2H), 7.92 (d, *J* = 8.6 Hz, 1H), 7.73–7.59 (m, 3H), 7.53–7.41 (m, 4H), 7.38–7.31 (m, 1H), 7.23 (t, *J* = 7.5 Hz, 1H), 7.06 (dd, *J* = 13.4, 5.5 Hz, 2H). TOF MS (EI⁺): C₂₁H₁₅NO₄S, found 377.07.

1-((4-Phenoxyphenyl)sulfonyl)-1H-indole-2-carboxylic acid (4)

Yield: white solid, 2.04 g, 26%. ¹H NMR (500 MHz, DMSO) δ: 11.73 (s, 1H), 8.08 (d, *J* = 9.0 Hz, 2H), 8.00 (d, *J* = 8.5 Hz, 1H), 7.68 (d, *J* = 8.0 Hz, 1H), 7.45 (q, *J* = 9.0 Hz, 3H), 7.21–7.37 (m, 3H), 7.09–7.15 (m, 4H). TOF MS (EI⁺): C₂₁H₁₅NO₅S, found 393.07.

1-((4-(tert-Pentyl)phenyl)sulfonyl)-1H-indole-2-carboxylic acid (5)

Yield: white solid, 2.37 g, 32%. ¹H NMR (500 MHz, DMSO) δ: 11.73 (s, 1H), 8.00 (t, *J* = 8.5 Hz, 3H), 7.67 (d, *J* = 7.5 Hz, 3H), 7.41–7.52 (m, 1H), 7.24–7.35 (m, 2H), 1.59 (q, *J* = 7.5 Hz, 2H), 1.22 (s, 6H), 0.54 (t, *J* = 7.5 Hz, 3H). TOF MS (EI⁺): C₂₀H₂₁NO₄S, found 371.12.

1-((4-Isobutoxyphenyl)sulfonyl)-1H-indole-2-carboxylic acid (6)

Yield: white solid, 1.72 g, 24%. ¹H NMR (500 MHz, DMSO) δ: 11.94 (s, 1H), 7.93 (d, *J* = 9.0 Hz, 2H), 7.82 (d, *J* = 8.0 Hz, 2H), 7.42 (s, 1H), 7.34–7.40 (m, 1H), 7.12 (d, *J* = 7.8 Hz, 2H), 6.86–6.93 (m, 1H), 4.69 (m, 1H), 1.29 (s, 6H). TOF MS (EI⁺): C₁₈H₁₇NO₅S, found 359.08.

General procedure for the preparation of compounds 7–12

The general procedure is illustrated immediately below with compound 7 as a specific example.

Synthesis of sodium 4-(benzyloxy)benzenesulfonate. To a suspension of sodium 4-hydroxybenzenesulfonate (1.96 g, 10 mmol), benzyl bromide (1.9 mL, 16 mmol), and NaOH (0.44 g, 11 mmol in 10 mL water) in isopropanol (25 mL). The mixture was stirred at 75°C for 20 h. After cooled to room temperature, the white solids that crystallized out of solution were filtered, washed with cold isopropanol. Yield: 1.9 g, 68%.

Synthesis of 4-(benzyloxy)benzenesulfonyl chloride. To a stirred suspension of sodium 4-(benzyloxy)benzenesulfonate (1.9 g, 6.8 mmol) in dry *N,N*-dimethylformamide (10 mL), dichloro sulfoxide (638 μ L, 8.8 mmol) was added dropwise at room temperature. After the reaction mixture was stirred for 5 min, poured onto ice, stirred further for 5 min and the precipitated white solid was filtered. The product was pure enough for next step without further purification. Yield: 1.7 g, 88%.

The amidation reaction and subsequent ester hydrolysis used same methods in compound 3.

1-((4-(Benzyloxy)phenyl)sulfonyl)-1H-indole-2-carboxylic acid (7)

Yield: white solid, 1.63 g, 40%. ^1H NMR (500 MHz, DMSO) δ : 11.94 (s, 1H), 8.08 (d, J = 9.0 Hz, 2H), 7.98 (d, J = 8.5 Hz, 1H), 7.65–7.78 (m, 5H), 7.58 (s, 1H), 7.45 (d, J = 8.0 Hz, 2H), 7.27–7.38 (m, 3H), 5.28 (s, 2H). TOF MS (EI^+): $\text{C}_{22}\text{H}_{17}\text{NO}_5\text{S}$, found 407.08.

1-((4-((2-Methylbenzyl)oxy)phenyl)sulfonyl)-1H-indole-2-carboxylic acid (8)

Yield: white solid, 1.47 g, 35%. ^1H NMR (500 MHz, DMSO) δ : 11.91 (s, 1H), 8.04 (d, J = 8.0 Hz, 1H), 7.96 (d, J = 9.0 Hz, 2H), 7.68 (d, J = 8.0 Hz, 2H), 7.42–7.52 (m, 2H), 7.31–7.39 (m, 2H), 7.15–7.29 (m, 4H), 5.16 (s, 2H), 2.28 (s, 3H). TOF MS (EI^+): $\text{C}_{23}\text{H}_{19}\text{NO}_5\text{S}$, found 421.10.

1-((4-((3-Methylbenzyl)oxy)phenyl)sulfonyl)-1H-indole-2-carboxylic acid (9)

Yield: white solid, 1.26 g, 30%. ^1H NMR (500 MHz, DMSO) δ : 11.92 (s, 1H), 8.06 (d, J = 8.0 Hz, 1H), 7.98 (d, J = 9.0 Hz, 2H), 7.43 (dt, J = 14.8, 6.5 Hz 4H), 7.19–7.28 (m, 4H), 7.08–7.12 (m, 2H), 5.16 (s, 2H), 2.30 (s, 3H). TOF MS (EI^+): $\text{C}_{23}\text{H}_{19}\text{NO}_5\text{S}$, found 421.10.

1-((4-((3,5-Dimethylbenzyl)oxy)phenyl)sulfonyl)-1H-indole-2-carboxylic acid (10)

Yield: white solid, 1.61 g, 37%. ^1H NMR (400 MHz, DMSO) δ : 11.92 (s, 1H), 8.03 (d, J = 8.4 Hz, 1H), 7.94 (d, J = 9.0 Hz, 2H), 7.68 (d, J = 7.8 Hz, 1H), 7.49 (t, J = 7.8 Hz, 1H), 7.35 (dd, J = 16.0, 8.4 Hz, 2H), 7.19 (d, J = 9.0 Hz, 2H), 6.99 (d, J = 7.4 Hz, 3H), 5.07 (s, 2H), 2.25 (s, 6H). TOF MS (EI^+): $\text{C}_{24}\text{H}_{21}\text{NO}_5\text{S}$, found 435.11.

1-((4-((3,4-Difluorobenzyl)oxy)phenyl)sulfonyl)-1H-indole-2-carboxylic acid (11)

Yield: white solid, 1.77 g, 40%. ^1H NMR (400 MHz, DMSO) δ : 13.58 (s, 1H), 8.00 (d, J = 9.0 Hz, 3H), 7.66 (d, J = 7.7 Hz, 1H), 7.50–7.58 (m, 1H), 7.40–7.49 (m, 2H), 7.31 (dd, J = 14.1, 6.9 Hz, 3H), 7.21 (d, J = 9.0 Hz, 2H), 5.15 (s, 2H). TOF MS (EI^+): $\text{C}_{22}\text{H}_{15}\text{F}_2\text{NO}_5\text{S}$, found 443.06.

1-((4-((3-chlorobenzyl)oxy)phenyl)sulfonyl)-1H-indole-2-carboxylic acid (12)

Yield: white solid, 1.76 g, 40%. ^1H NMR (500 MHz, DMSO) δ : 11.71 (s, 1H), 7.99 (d, J = 7.5 Hz, 2H), 7.65 (t, J = 8.9 Hz, 1H), 7.51 (s, 1H), 7.43 (dt, J = 14.8, 6.2 Hz 4H), 7.31 (t, J = 7.5 Hz, 1H),

7.17–7.28 (m, 3H), 7.03–7.10 (m, 1H), 5.18 (s, 2H). TOF MS (EI^+): $\text{C}_{22}\text{H}_{16}\text{ClNO}_5\text{S}$, found 441.04.

^1H - ^{15}N HSQC

^1H - ^{15}N HSQC spectra were recorded for 0.1 mM ^{15}N -labeled Mcl-1. Inhibitor solution was added at a 2:1 ratio. The ^1H - ^{15}N HSQC spectra were recorded on a Bruker Advance DRX600 MHz spectrometer, processed by NMRPipe and visualized by NmrViewJ 8.0. Chemical shift changes were calculated as $[(\Delta^1\text{H ppm})^2 + (0.2 \times \Delta^{15}\text{N ppm})^2]^{1/2}$ as a function of the residue number.

Molecular docking

Molecular modeling was performed with AutoDock 4.0. The 3D structures of the human Mcl-1 (hMcl-1; PDB ID: 2PQK) was obtained from the Protein Data Bank. The 3D structures of the inhibitors were generated using Chembio3D Ultra 11.0 followed by energy minimization. Grid maps covering residues that were perturbed more than the threshold value of 0.1 ppm in the BH3 binding groove of the proteins were defined for all inhibitors in the AutoDock calculations using a grid spacing of 0.375 Å. The GA-LS algorithm was adopted using default settings. For each docking job, 100 hybrid GA-LS runs were carried out. A total of 100 possible binding conformations were generated and grouped into clusters based on a 1.0 Å cluster tolerance. The docking models were analyzed and represented using PyMol molecular graphics system.

Pharmacology

Fluorescence polarization-based binding assay (FPA)

For the competitive binding assay for Mcl-1 protein, FAM-Bid peptide (10 nM) and Mcl-1 protein (55 nM) were preincubated in the assay buffer (25 mM Tris, pH 8.0; 150 mM NaCl). Next, serial dilutions of compounds were added. After a 1-min incubation, the polarization values were measured using the Spectra Max M5 Detection System in a black 96-well plate. Free peptide controls (fluorescent peptide only) and bound peptide controls (fluorescent peptide in the presence of Mcl-1) were included on each assay plate. The percentage of inhibition was derived from the equation: % inhibition = $100 \times (1 - (\text{mP} - \text{mPf}) / (\text{mPb} - \text{mPf}))$ in which mPf is the free peptide control and mPb is the bound peptide control. The computer program for calculating K_i values for FPA-based assays is available free of charge at: http://sw16.im.med.umich.edu/software/calc_Ki/.

Western blot

After cells were lysed in NP-40 lysis buffer and centrifuged, the supernatant was subjected to Western blot by using specific antibody. Electrophoresis and transfer to membrane were performed routinely. Protein signals were detected by the ECL method (Amersham Pharmacia Biotech).

Apoptosis assay

Phosphatidylserine (PS) exposure was quantified by surface Annexin V-FITC staining. Cells were seeded in each well of 6-

well tissue culture plates and treated with compounds for 48 h after 24 h. Cells were washed twice with PBS and incubated with a 1:40 solution of FITC-conjugated Annexin V for 10 min at room temperature. Stained cells were analyzed by flow cytometry.

This work was supported by the National Natural Science Foundation of China (21372036, 81570129, 81430083, 21502015, and 21402022).

The authors have declared no conflict of interest.

References

- [1] R. M. Brady, A. Vom, M. J. Roy, B. J. Smith, R. M. Moss, E. Hatzis, D. C. S. Huang, J. P. Parisot, I. P. Street, G. Lessen, *J. Med. Chem.* **2014**, *57*, 1323–1343.
- [2] S. Cory, D. C. S. Huang, J. M. Adams, *Oncogene* **2003**, *22*, 8590–8607.
- [3] M. Vogler, D. Dinsdale, M. J. S. Dyer, G. M. Cohen, *Cell Death Differ.* **2009**, *16*, 360–367.
- [4] E. F. Lee, P. E. Czabotar, B. J. Smith, K. Zobel, M. Colman, W. D. Fairlie, *Cell Death Differ.* **2007**, *14*, 1711–1713.
- [5] B. E. Sleebs, W. J. A. Kersten, S. Kulasegaram, G. Nikolakopoulos, E. Hatzis, R. M. Moss, J. P. Parisot, H. Yang, L. Chen, G. Lessene, *J. Med. Chem.* **2013**, *56*, 5514–5540.
- [6] P. H. Bernardo, T. Sivaraman, K. Wan, J. Xu, J. Krishnamoorthy, J. S. F. Chin, D. S. W. Lim, C. L. L. Chai, *J. Med. Chem.* **2010**, *53*, 2314–2318.
- [7] G. Lessene, P. E. Czabotar, P. M. Colman, *Nat. Rev. Drug Discov.* **2008**, *7*, 989–1000.
- [8] M. R. Arkin, J. A. Wells, *Nat. Rev. Drug Discov.* **2004**, *3*, 301–317.
- [9] C. Tse, A. R. Shoemaker, J. Adickes, M. G. Anderson, J. Chen, S. Jin, E. F. Johnson, K. C. Marsh, M. J. Mitten, S. W. Elmore, *Cancer Res.* **2008**, *68*, 3421–3428.
- [10] W. H. Wilson, O. A. O'Connor, M. S. Czuczman, A. S. LaCasce, J. F. Gerecitano, J. P. Leonard, A. Tulpule, K. Dunleavy, H. Xiong, R. A. Humerickhouse, *Lancet Oncol.* **2010**, *11*, 1149–1159.
- [11] M. F. van Delft, A. H. Wei, K. D. Mason, C. J. Vandenberg, L. Chen, P. E. Czabotar, S. N. Willis, C. L. Scott, C. L. Day, S. Cory, D. C. S. Huang, *Cancer Cell* **2006**, *10*, 389–399.
- [12] D. Yecies, N. E. Carlson, J. Deng, A. Letai, *Blood* **2010**, *115*, 3304–3313.
- [13] M. R. Warr, G. C. Shore, *Curr. Mol. Med.* **2008**, *8*, 138–147.
- [14] L. Chen, M. E. Lanning, S. Fletcher, *Austin J. Anal. Pharm. Chem.* **2014**, *1*, 1015–1020.
- [15] K. Doi, R. Li, S. Sung, H. Wu, Y. Liu, W. Manieri, G. Krishnegowda, A. Awwad, A. Dewey, X. Liu, S. Amin, C. Cheng, Y. Qin, E. Schonbrunn, S. Sebti, H. Wang, *J. Biol. Chem.* **2012**, *287*, 10224–10235.
- [16] M. N. Schulz, R. E. Hubbard, *Curr. Opin. Pharmacol.* **2009**, *9*, 615–621.
- [17] M. Orita, K. Ohno, T. Niimi, *Drug Discov. Today* **2009**, *14*, 321–328.
- [18] H. Chen, X. Zhou, A. Wang, Y. Zheng, Y. Gao, J. Zhou, *Drug Discov. Today* **2015**, *20*, 105–113.
- [19] T. Oltersdorf, S. W. Elmore, A. R. Shoemaker, R. C. Armstrong, D. J. Augeri, B. A. Belli, M. Bruncko, T. L. Deckwerth, J. Dinges, K. J. Tomaselli, B. Wang, M. D. Wendt, H. Zhang, S. W. Fesik, S. H. Rosenberg, *Nature* **2005**, *435*, 677–681.
- [20] S. B. Shuker, P. J. Hajdilk, R. P. Meadows, S. W. Fesik, *Science* **1996**, *274*, 1531–1534.
- [21] D. A. Erlanson, R. S. McDowell, T. O'Brien, *J. Med. Chem.* **2004**, *47*, 3463–3482.
- [22] S. Schultes, C. Graaf, E. E. J. Haaksma, I. J. P. Esch, R. Leurs, O. Kramer, *Drug Discov. Today* **2010**, *7*, 157–162.
- [23] R. A. E. Carr, M. Congreve, C. W. Murray, D. C. Rees, *Drug Discov. Today* **2005**, *10*, 987–992.
- [24] P. J. Hajduk, *J. Med. Chem.* **2006**, *49*, 6972–6976.
- [25] E. F. Lee, P. E. Czabotar, M. F. van Delft, E. M. Michalak, M. J. Boyle, S. N. Willis, H. Puthalakath, P. Bouillet, P. M. Colman, D. C. S. Huang, W. D. Fairlie, *J. Cell Biol.* **2008**, *180*, 341–355.
- [26] P. E. Czabotar, E. F. Lee, M. F. van Delft, C. L. Day, B. J. Smith, D. C. S. Huang, W. D. Fairlie, M. G. Hinds, P. M. Colman, *PNAS* **2007**, *104*, 6217–6222.
- [27] A. Friberg, D. Vigil, B. Zhao, R. N. Daniels, J. P. Burke, P. M. Garcia-Barrantes, D. Camper, B. A. Chauder, T. Lee, E. T. Olejniczak, S. W. Fesik, *J. Med. Chem.* **2013**, *56*, 15–30.
- [28] J. Basset, M. Romero, T. Serra, M. D. Pujol, *Tetrahedron* **2012**, *68*, 356–362.
- [29] R. G. Schult, *J. Org. Chem.* **1961**, *26*, 5195–5196.
- [30] P. M. O'Brien, D. F. Ortwine, A. G. Pavlovsky, J. A. Picard, D. R. Sliskovic, B. D. Roth, R. D. Dyer, L. L. Johnson, C. F. Man, H. Hallak, *J. Med. Chem.* **2000**, *43*, 156–166.
- [31] E. Nuti, S. Santamaria, F. Casalini, K. Yamamoto, L. Marinelli, V. L. Pietra, E. Novellino, E. Orlandini, S. Nencetti, A. M. Marini, S. Salerno, S. Taliani, F. D. Settimo, H. Nagase, A. Rossello, *Eur. J. Med. Chem.* **2013**, *62*, 379–394.
- [32] M. I. Attia, M. Timmermann, P. Högger, C. Herdeis, *Eur. J. Org. Chem.* **2007**, *22*, 3669–3675.